PCCP

PAPER

Magnetic and thermodynamic properties of face-centered cubic Fe–Ni alloys

Cite this: *Phys. Chem. Chem. Phys.*, 2014, **16**, 16049

M. Yu. Lavrentiev,* J. S. Wróbel, D. Nguyen-Manh and S. L. Dudarev

Received 28th March 2014,
Accepted 2nd June 2014

DOI: 10.1039/c4cp01366b

www.rsc.org/pccp

A model lattice *ab initio* parameterized Heisenberg–Landau magnetic cluster expansion Hamiltonian spanning a broad range of alloy compositions and a large variety of chemical and magnetic configurations has been developed for face-centered cubic Fe–Ni alloys. The thermodynamic and magnetic properties of the alloys are explored using configuration and magnetic Monte Carlo simulations over a temperature range extending well over 1000 K. The predicted face-centered cubic–body-centered cubic coexistence curve, the phase stability of ordered Fe_3Ni, FeNi, and $FeNi_3$ intermetallic compounds, and the predicted temperatures of magnetic transitions simulated as functions of alloy composition agree well with experimental observations. Simulations show that magnetic interactions stabilize the face-centered cubic phase of Fe–Ni alloys. Both the model Hamiltonian simulations and *ab initio* data exhibit a particularly large number of magnetic configurations in a relatively narrow range of alloy compositions corresponding to the occurrence of the Invar effect.

1. Introduction

Developing structural materials that retain their engineering properties over extended periods of time at high temperatures and high radiation dose is one of the major challenges for fusion and fission materials science and technology. Developing simulation algorithms for modelling such materials, particularly steels, is one of the objectives of the European fusion programme.[1] Face-centered cubic (fcc) Fe–Ni–Cr based austenitic steels retain good engineering strength at high temperatures, making them attractive candidate materials for fusion and advanced fission technology. In particular, austenitic 304 and 316 steels are used as structural materials for light water and fast breeder fission reactors. These steels contain about 10 at% Ni and 20 at% Cr,[2,3] so that any methodology for modelling such steels should in the first place be able to model ternary Fe–Ni–Cr alloys in the composition range where neither of the constituent elements can be treated as impurity. An extra factor that must be taken into account when modelling iron-based alloys and steels is the fact that the phase stability of iron-based alloys is controlled by magnetism, for example, magnetism stabilizes the ferritic body-centered cubic (bcc) phase of pure iron under ambient conditions. The existing theoretical treatments of the phase diagram of the Fe–Ni system are based on interatomic interaction potentials[4–7] and so are unable to describe magnetic phase transitions in that system.

Magnetic Cluster Expansion (MCE) simulations of Fe–Cr alloys[8–11] showed that a model based on an *ab initio* parameterized Heisenberg–Landau MCE Hamiltonian was able to describe a broad range of magnetic and structural transformation effects in bcc iron-based magnetic alloys. This has prompted us to develop an MCE parameterization for fcc Fe–Ni alloys as a step towards the treatment of ternary Fe–Ni–Cr alloys. The phase diagram of binary Fe–Ni alloys[12] shows that the solubility of Ni in bcc iron is very low, as opposite to the high solubility of Ni in fcc Fe, where the two species are fully soluble in the entire range of concentrations at high temperature. Hence a realistic MCE Hamiltonian should be expected to be able to describe the miscibility gap between fcc Fe–Ni, bcc Fe and bcc Fe–Ni. Another important feature of the phase diagram is the presence of an ordered $L1_2$ structure with $FeNi_3$ composition. Also, the possible occurrence of ordered FeNi and Fe_3Ni compounds (the first of which was found in meteorites[13–15]) should be explored.

This paper is organized as follows. In Section 2, we parameterize the Heisenberg–Landau MCE Hamiltonian for the fcc Fe–Ni alloy. The magnetic properties of pure fcc iron and nickel and their solid solutions are investigated in Section 3, and the phase diagram of the system is explored in Section 4. We summarize the results of our study and conclude in Section 5.

2. Parameterization of magnetic cluster expansion

The main principles of MCE are described in ref. 8, 9 and 16. The complete functional form of the Heisenberg–Landau

CCFE, Culham Science Centre, Abingdon, Oxon, OX14 3DB, UK.
E-mail: Mikhail.Lavrentiev@ccfe.ac.uk

Hamiltonian used for MCE simulations is:

$$
\begin{aligned}
H(\{\sigma_i\},\{\mathbf{M}_i\}) \;=\; & \sum_{ij\in 1\mathrm{NN}} I^{(1\mathrm{NN})}\sigma_i\sigma_j + \sum_{ij\in 2\mathrm{NN}} I^{(2\mathrm{NN})}\sigma_i\sigma_j \\
& + \sum_{ij\in 3\mathrm{NN}} I^{(3\mathrm{NN})}\sigma_i\sigma_j + \sum_{ij\in 4\mathrm{NN}} I^{(4\mathrm{NN})}\sigma_i\sigma_j \\
& + \sum_i \left(A_0 + A_1\sigma_i + \sigma_i \left(A_2^{(1\mathrm{NN})} \sum_{j\in 1\mathrm{NN}} \sigma_j + A_2^{(2\mathrm{NN})} \right.\right. \\
& \left.\left. \times \sum_{j\in 2\mathrm{NN}} \sigma_j + A_2^{(3\mathrm{NN})} \sum_{j\in 3\mathrm{NN}} \sigma_j \right) \right) \mathbf{M}_i^2 \\
& + \sum_i \left(B_0 + B_1\sigma_i + \sigma_i \left(B_2^{(1\mathrm{NN})} \sum_{j\in 1\mathrm{NN}} \sigma_j + B_2^{(2\mathrm{NN})} \right.\right. \\
& \left.\left. \times \sum_{j\in 2\mathrm{NN}} \sigma_j + B_2^{(3\mathrm{NN})} \sum_{j\in 3\mathrm{NN}} \sigma_j \right) \right) \mathbf{M}_i^4 \\
& + \sum_i (C_0 + C_1\sigma_i)\mathbf{M}_i^6 + \sum_i (D_0 + D_1\sigma_i)\mathbf{M}_i^8 \\
& + \sum_{ij\in 1\mathrm{NN}} J^{(1\mathrm{NN})}_{\sigma_i\sigma_j}\mathbf{M}_i\cdot\mathbf{M}_j + \sum_{ij\in 2\mathrm{NN}} J^{(2\mathrm{NN})}_{\sigma_i\sigma_j}\mathbf{M}_i\cdot\mathbf{M}_j \\
& + \sum_{ij\in 3\mathrm{NN}} J^{(3\mathrm{NN})}_{\sigma_i\sigma_j}\mathbf{M}_i\cdot\mathbf{M}_j + \sum_{ij\in 4\mathrm{NN}} J^{(4\mathrm{NN})}_{\sigma_i\sigma_j}\mathbf{M}_i\cdot\mathbf{M}_j
\end{aligned}
\tag{1}
$$

Here, spin-like variables σ_i refer to the chemical nature of an atom occupying lattice site i and take values +1 for Fe and −1 for Ni. The Is are the non-magnetic cluster expansion coefficients; parameters As and Bs represent Landau coefficients for the quadratic and quartic magnetic self-energy terms, respectively, which depend on the local environment of each atom; and Cs and Ds are, respectively, the 6th and 8th order coefficients which we have chosen to be independent of the environment. A reason for extending the on-site Landau expansion to the 8th order in magnetic moment is discussed below. The Js are the inter-lattice-site Heisenberg magnetic interaction parameters. The functional form of the MCE Heisenberg–Landau Hamiltonian (1) guarantees that the magnetic self-energy terms, and hence the directions and magnitudes of atomic magnetic moments $\mathbf{M}_i$ predicted by the model, depend on the local environment of each atom in the alloy. Hamiltonian (1) is based on the undistorted rigid lattice approximation, which is valid for Fe–Ni alloys where the atomic radii of the two elements are similar (see, *e.g.*, Table 1 in ref. 17). We note that the functional form of Hamiltonian (1) involves the Landau expansion for magnetic self-energy that is extended beyond the quadratic and quartic terms. Below we show that such an extension is actually necessary for the treatment of magnetic properties of fcc Fe–Ni alloys.

Whereas Hamiltonian (1) can be parameterized in several different ways, still the search for a suitable set of Landau and Heisenberg parameters always begins by selecting a set of ordered structures, the energies and magnetic moments of which are calculated *ab initio*. In the fcc Fe–Ni alloy case, a set of 29 binary configurations was investigated by *ab initio* density functional theory (DFT) calculations, together with the two limiting cases of pure fcc iron and fcc nickel. Spin-polarized DFT calculations were performed using the projector augmented wave (PAW) method[18] implemented in the VASP package.[19–21] Exchange–correlation was treated within the generalized gradient approximation GGA-PBE.[22] The total energies and magnetic moments were calculated assuming the plane-wave cutoff energy of 400 eV and a k-point mesh with spacing of 0.26 Å^{-1}.

An *ab initio* investigation of ferromagnetic fcc iron shows the occurrence of two, so-called high-spin and low-spin magnetic states. The high-spin configuration is slightly more energetically favourable than the low-spin one. However the difference is of the order of ∼10 meV per atom, with the result that both configurations contribute equally significantly to finite temperature magnetic properties. The occurrence of high- and low-spin magnetic configurations in the ground state of the alloy cannot be accounted for by a Landau-type Hamiltonian involving only the quadratic and quartic terms, since such a functional form of the Hamiltonian exhibits only one minimum as a function of the magnitude of the magnetic moment vector. In order to describe both the high- and low-spin magnetic configurations of fcc Fe, it is necessary to include terms up to the 8th order in magnetic moment in the Landau expansion. We use DFT data to fit the energy of pure fcc ferromagnetic Fe as a function of magnetic moment. Fig. 1 shows that an 8th order magnetic moment Landau expansion agrees well with *ab initio* results, replicating the correct difference between the energies of low-spin and high-spin magnetic configurations. For consistency, the Landau expansion (see Hamiltonian (1)) was extended to the 8th order term also for the nickel atoms.

Before discussing how to fit interaction parameters I and J, it is important to note that in our implementation of the MCE they are independent of the volume of the system. It is well established that the magnetic properties of Fe–Ni alloys strongly depend on both volume and alloy composition.[23,24] The parameters of the cluster expansion method developed by Sanchez *et al.*[25] either can be concentration- and volume-dependent, or can be fitted to the equilibrium (volume-relaxed) quantum-mechanical energy and be

Table 1 Magnetic Heisenberg interaction parameters $J_{\sigma_i\sigma_j}$ and non-magnetic interaction parameters I (in meV) fitted to *ab initio* data and used in MCE simulations

	$J_{\mathrm{Fe-Fe}}$	$J_{\mathrm{Fe-Ni}}$	$J_{\mathrm{Ni-Ni}}$	I
1st nearest neighbour	−0.793072	1.515864	−13.153009	−13.30043
2nd nearest neighbour	−10.827175	−2.709532	7.227536	6.902392
3rd nearest neighbour	0.546719	−2.500082	−5.604799	0.208886
4th nearest neighbour	2.305911	1.649425	−6.744045	−1.160406

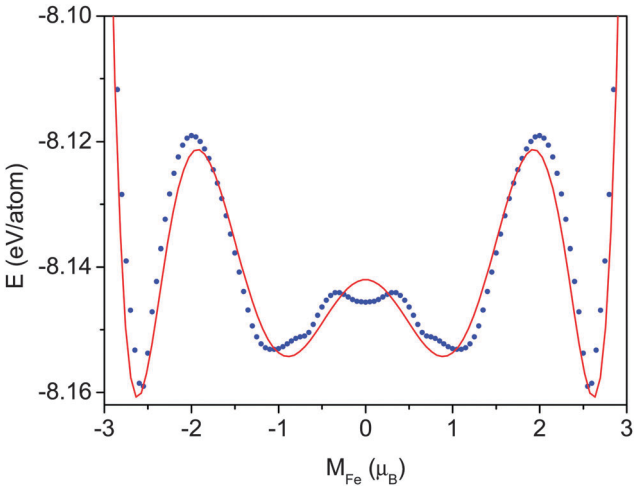

Fig. 1 Comparison of DFT (points) energies of ferromagnetic fcc Fe plotted as a function of magnetic moment and the MCE Landau expansion (line), which includes terms up to the 8th order in atomic magnetic moment.

volume-independent. The two approaches are equivalent and their choice is a matter of convenience.[25,26] For example, a recent non-magnetic cluster expansion study of Fe–Ni, Fe–Pd, and Fe–Pt by Barabash *et al.*,[27] based on volume- and concentration-independent parameters, resulted in a successful prediction of several previously unknown stable structures of those compounds. One of those structures, the Z1 Fe_3Ni superlattice, was found to be more stable than the $L1_2$ structure, as was noted previously (we discuss those phases below, see Section 3.3). In our work, we use volume-independent interaction parameters obtained from fully relaxed *ab initio* calculations. Also, the concentration dependence of our MCE implementation is partly described by the on-site Landau terms A and B in Hamiltonian (1), since these terms depend on the local environment of each atom.

In an earlier MCE study of bcc–fcc transitions in Fe and Fe–Cr alloys, we showed that extending the range of Heisenberg interaction parameters to the third nearest neighbour was sufficient for modelling magnetic configurations in pure fcc iron.[9] When fitting the Heisenberg parameters to the Fe–Ni system, we found that it was necessary to extend the range up to the fourth nearest neighbour in order to describe the Ni–Ni and Ni–Fe interactions. Hence, to retain consistency, we decided to extend the range of magnetic and non-magnetic parameters to the 4th nearest neighbour for the Fe–Fe interactions as well. For each of the 29 ordered configurations, as well as for pure nickel and iron, the *ab initio* energy data (including, for pure iron, several ferro- and antiferromagnetic configurations) were used to evaluate a trial set of MCE parameters. Also, the derivatives of the MCE energy with respect to magnetic moments were calculated numerically. The sum of squares of deviations of MCE predictions from the DFT data,

$$S = \sum_m \alpha_m \left(E_m^{\mathrm{DFT}} - E_m^{\mathrm{MCE}}\right)^2 + \sum_m \beta_m \sum_n \left(\frac{\partial E_m^{\mathrm{MCE}}}{\partial \mathbf{M}_n}\right)^2 \qquad (2)$$

was taken as a measure of goodness of an MCE fit. Here, the index m numbers structures, and the index n runs through all the atoms in an ordered structure m. The above equation includes both the differences between the MCE and DFT energies, and also a measure of deviation of the position of the energy minimum predicted by MCE from its DFT minimum value, characterized by the sum of squares of derivatives of the MCE energy with respect to atomic magnetic moments. The coefficients α_m and β_m were adjusted during the fitting procedure to reflect contributions of various configurations to the fit and are, in general, chosen to be larger for the lower energy configurations. The values of magnetic Heisenberg interaction parameters J and the non-magnetic interaction parameters I derived using eqn (2) are given in Table 1, and the on-site Landau expansion coefficients A, B, C, and D are given in Table 2. DFT and MCE energies of mixing for the structures included in the fit are compared in Fig. 2. The mean square deviation of *ab initio* energies from those predicted by MCE is 12 meV.

Table 2 On-site Landau expansion terms (in meV) used in MCE simulations. Numbers 0, 1, and 2 stand for the lower index; (1NN), (2NN), and (3NN) stand for the upper index in the Hamiltonian (1)

	0	1	2 (1NN)	2 (2NN)	2 (3NN)
A	−66.931806	−15.682389	3.38505	3.656047	0.794464
B	245.865553	−213.470278	0.10439	−0.2039	−0.140469
C	−10.149505	3.655495			
D	9.614085	−9.185915			

Monte Carlo simulations of pure Fe and Ni and Fe–Ni alloys were performed as follows. The simulation box contained 16 384 atoms ($16 \times 16 \times 16$ fcc unit cells, each containing 4 atoms). For the chemically ordered structures, at each Monte Carlo step a trial random change in magnetic moment of a randomly chosen atom was attempted and accepted or rejected according to the Metropolis criterion. Both the thermalization and accumulation stages included 40 000 attempts per atom. For the low temperature cases and complex magnetic structures of pure iron, simulations involving 130 000 attempts per atom were also performed to ensure that the system has reached equilibrium. For the case of

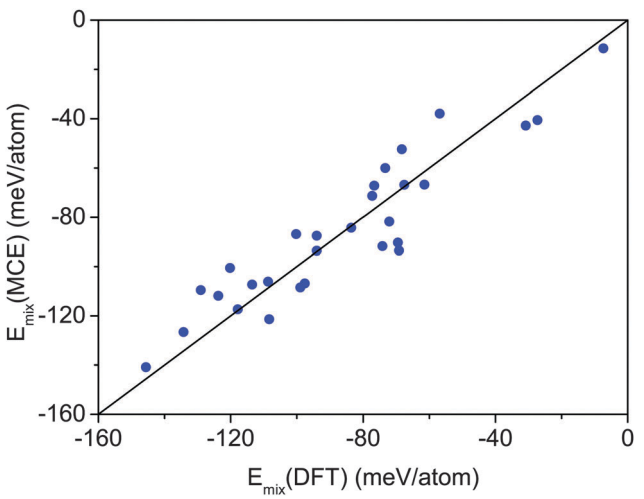

Fig. 2 Comparison of DFT and MCE energies of mixing for the alloy configurations used for fitting the MCE Hamiltonian.

random structures, we used two types of simulations. The first was similar to the one used for the ordered alloys, but with random configurations corresponding to a given Fe and Ni content. In comparison with *ab initio* calculations, where the relatively small size of the simulation cell requires using special quasi-random structures (SQS) (see, *e.g.*, ref. 28), large-scale Monte Carlo simulations can be performed by choosing random configurations for the two types of atoms. In order to verify the results, several comparisons with other random structures were made by changing the seed of the random number generator. Thermodynamic data obtained in this way correspond to a completely random system and are hence characterized by the known value of configurational entropy.

$$S_{\mathrm{conf}} = k_{\mathrm{B}}(x_{\mathrm{Fe}} \ln(x_{\mathrm{Fe}}) + (1 - x_{\mathrm{Fe}})\ln(1 - x_{\mathrm{Fe}})) \qquad (3)$$

Another approach is the exchange Monte Carlo, in which trial changes in magnetic moment are combined with attempts to exchange two randomly chosen atoms of different species. This approach was previously successfully used in Monte Carlo simulations based on interatomic interaction potentials,[29–32] as well as on the non-magnetic cluster expansion.[33] It gives reliable results for the enthalpy of mixing, but the configurational entropy and thus the free energy of mixing is difficult to evaluate. By comparing the enthalpies of mixing obtained using the two approaches, we estimate how significantly a given configuration of the alloy deviates from a completely random mixture.

3. Magnetic and thermodynamic properties

3.1 Magnetism of pure Fe and Ni

For pure fcc iron, the first and second nearest-neighbour Heisenberg magnetic interaction parameters favour ferromagnetic ordering of moments, whereas the third and the fourth favour antiferromagnetic ordering (see Table 1). An interplay between these interactions results in that the lowest-energy magnetic configuration is non-collinear antiferromagnetic. The energies of several magnetic configurations of fcc iron are shown and compared with DFT results in Table 3. The predicted non-collinear magnetic ground state agrees with the findings derived from our MCE study of bcc–fcc transitions in Fe and Fe–Cr alloys,[9] even though the set of MCE parameters used here is different from that used in ref. 9. Non-collinear antiferromagnetic ordering of magnetic moments was experimentally discovered at low temperatures in fcc Fe precipitates embedded in a Cu matrix.[34,35] Non-collinear magnetism is realised in magnetic materials with competing magnetic coupling parameters, where magnetic interactions are comparable in terms of their magnitude and change sign as a function of interatomic distance. In earlier studies of fcc Fe–Cr, the nearest neighbour Fe–Fe interaction was taken as ferromagnetic, whereas the second and third nearest neighbour Fe–Fe interaction parameters were antiferromagnetic (ref. 9, Table 1). In the MCE Hamiltonian used here, extending the Landau expansion to the 8th order in magnetic moment to model the high-spin and low-spin magnetic states resulted in the increase of the magnitude of the (negative, ferromagnetic) second order magnetic term. In our fit this corresponds to the strongly ferromagnetic second nearest neighbour interactions. Although the antiferromagnetic 3rd and 4th nearest neighbour interaction parameters are smaller in terms of their magnitude (see Table 1), the relatively large number of the third (24 atoms) and fourth (12 atoms) nearest neighbours in the fcc lattice is sufficient to overwhelm the effect of ferromagnetic interactions involving only six second nearest neighbours. As a result, the antiferromagnetically ordered single and double layer structures have energies lower than that of the ferromagnetic configuration. Still, the ground state antiferromagnetic collinear configuration of fcc Fe turns out to be magnetically frustrated, and the frustration is partially resolved by rotating the magnetic moments away from collinearity. We observed similar behaviour of magnetic moments in both *ab initio* and MCE studies of Fe–Cr interfaces in the bcc lattice.[36]

While the total magnetic moment of the alloy is zero due to averaging over all the possible directions of atomic magnetic moments, the average magnitude of the magnetic moment vector of an individual Fe atom $\langle|\mathbf{M}|\rangle = \frac{1}{N}\sum_{i=1}^{N}|\mathbf{M}_i|$ does not vanish. The slightly lower energy of the high-spin state compared to the low-spin one ensures that at low temperatures the average magnitude of atomic magnetic moment is of the order of 2.648 μ_{B}. As temperature increases, the slope of energy variation as a function of temperature changes at about 450 K (Fig. 3),

Table 3 Energies of several magnetic configurations of fcc iron (meV per atom) found in MCE and DFT calculations. The values of the energies are given with respect to the energy of a non-magnetic state

	MCE	DFT
Non-magnetic	0	0
Low-spin ferromagnetic	−12	−5
High-spin ferromagnetic	−19	−14
Single layer antiferromagnetic	−51	−39
Double layer antiferromagnetic	−51	−60
Non-collinear antiferromagnetic	−53	

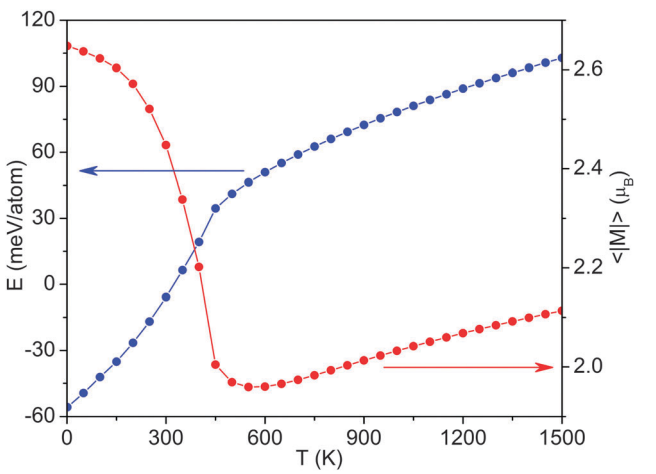

Fig. 3 Temperature dependence of the energy (blue, left *Y*-axis) and the average length of atomic magnetic moment (red, right *Y*-axis) of pure fcc iron.

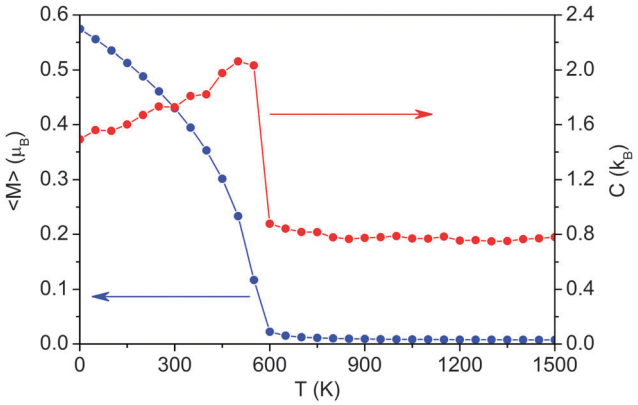

Fig. 4 Temperature dependence of magnetic moment (blue, left *Y*-axis) and the magnetic part of the specific heat of pure fcc nickel (red, right *Y*-axis).

indicating a transition from an antiferromagnetic to a paramagnetic state. This temperature is higher than that found using the parameterization given in ref. 9, though the Néel temperature is still very low compared to the temperature range of stability of fcc iron (1185–1667 K[37]). Below the magnetic transition the average magnitude of an atomic magnetic moment decreases as a function of temperature due to the mixing of high-spin and low-spin magnetic states, eventually decreasing to 2 μ_B. Above the transition, where the moments are completely disordered, the average length of the magnetic moment $\langle|\mathbf{M}|\rangle$ increases slowly as a function of temperature, see Fig. 3.

For pure fcc nickel, Monte Carlo simulations predict strong collinear ferromagnetic ordering at low temperatures, in agreement with experiment and *ab initio* calculations. This can also be deduced from the set of MCE parameters given in Table 1, where for almost all the neighbours the Heisenberg interaction parameters are ferromagnetic. The low-temperature value of atomic magnetic moment found in MCE simulations, 0.575 μ_B, is within 5% of the experimentally observed value of 0.605 μ_B.[38] Thermal fluctuations destroy magnetic order at 550–600 K according to the magnetic moment data shown in Fig. 4. This agrees well with the experimental Curie temperature of nickel of 631 K,[38] confirming the good accuracy of our MCE parameter set. For comparison, recent theoretical studies of the Curie temperature of Ni[39,40] predicted temperatures which are much farther away from the experiment: 300 K deduced from Monte Carlo simulations, 369 K found using the random-phase approximation, and 413 K found using a mean-field approximation (see ref. 39, Table 1). Only the renormalized random-phase approximation[39] predicted the Curie temperature of 686 K comparable with our results. The occurrence of a magnetic phase transition just below 600 K is also confirmed by the clearly pronounced maximum in the temperature dependent magnetic part of the specific heat shown in Fig. 4.

3.2 Magnetism and the enthalpy of mixing of Fe–Ni alloys

Experimental and theoretical data on the enthalpy of mixing of Fe–Ni alloys are relatively scarce. A recent study by Idczak *et al.*[41] was performed using alloy samples with iron content below 10 at% where the data were subsequently extrapolated to the entire range of alloy compositions. Their results exhibit negative enthalpy of mixing with a minimum of approximately 70 meV per atom, whereas in the interatomic potential studies[6] a much smaller minimum value of about 40 meV per atom was found. Our results regarding the enthalpies of mixing, computed assuming random alloy configurations, are shown in Fig. 5. The reference energies at the limits of the composition range (pure Fe and pure Ni) were taken as those of ground state magnetic configurations, *i.e.* non-collinear antiferromagnetic for Fe and ferromagnetic for Ni. The minimum value of the enthalpy of mixing is close to −100 meV per atom, which is lower than what is found in ref. 41. However, this prediction is in good agreement with our own DFT calculations, which exhibit even lower enthalpies of mixing for several ordered structures (see Fig. 2). With increasing temperature the absolute value of the enthalpy of mixing increases slightly, as shown in Fig. 5. Even lower negative enthalpies of mixing are found in simulations, where exchanges between atoms are allowed upon decreasing the temperature, thus allowing the system to find the lowest-energy chemical and magnetic configurations. Fig. 6 shows the result of such a simulation, where the minimum value of the enthalpy of mixing is as low as −130 meV per atom. Enthalpies of formation acquire much higher values at the Fe end of the concentration range, because bcc iron has lower energy than fcc Fe. Our DFT calculations predict that the formation energy of ferromagnetic bcc Fe is 107 meV per atom lower than the lowest energy antiferromagnetic double layer configuration of fcc Fe.

When exploring the magnetic moment of a randomly mixed system, we found that magnetic structures differ strongly between high- and low-Ni concentration limits. As shown in Section 3.1, the ground state of pure fcc Fe is non-collinear antiferromagnetic. At small nickel content, the system remains non-collinear antiferromagnetic. Emergence of a non-zero total magnetic moment marking the transition from antiferromagnetism to non-collinear ferromagnetism in our model takes

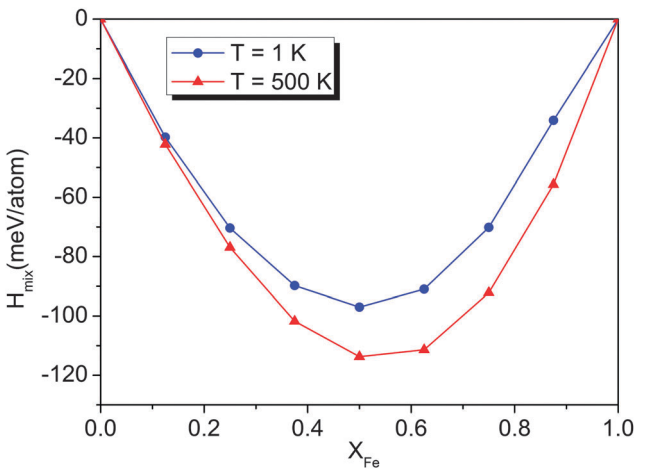

Fig. 5 Enthalpy of mixing computed for random fcc Fe–Ni alloy configurations at low and high temperatures T = 1 K and T = 500 K.

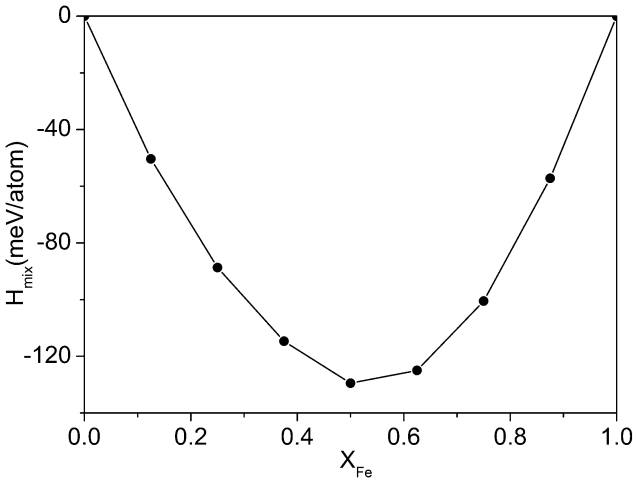

Fig. 6 Enthalpy of mixing of fcc Fe–Ni alloys plotted as a function of Fe content for configurations obtained by allowing atom exchanges.

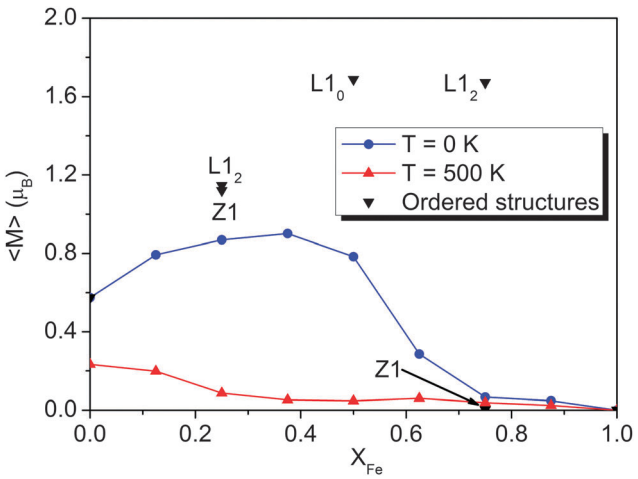

Fig. 7 The total magnetic moment of a random fcc Fe–Ni mixture plotted as a function of Fe content at a very low temperature and at T = 500 K. Also, magnetic moments of several ordered structures are shown, as described in the text.

place at around 25 at% Ni, as shown in Fig. 7. This result is in good agreement with the magnetic phase diagrams of the Fe–Ni system recently constructed by Cacciamani *et al.*[42] and Xiong *et al.*,[43] who used extensive experimental data and *ab initio* calculations, supplemented by CALPHAD modelling. This transition is not accompanied by large changes in the energy of the system, hence several very different magnetic configurations compete within a narrow range of energies. In order to find the magnetic ground state of the random configurations in the 25–50 at% interval of Ni concentrations, we performed three-stage quenching for each concentration studied, namely (1) from 1000 K to 1 K, (2) from 1 K to 0.001 K, and (3) from 0.001 K to 10^{-6} K. It is also worth mentioning that the magnetic behaviour of the alloy changes from antiferromagnetic to non-collinear ferromagnetic at concentrations close to those of the Invar alloy (~35 at% Ni), confirming the applicability of the MCE model to simulating even fairly subtle details of magnetic properties of this alloy system.

With increasing Ni content, the relatively strong ferromagnetic interactions between Fe and Ni atoms result in the magnetic configuration of random Fe–Ni alloys approaching collinearity at the nickel content above 50 at%. The system becomes ferromagnetic and almost completely collinear at 75 at% Ni and above. Because the magnetic moment of Fe is much larger than that of Ni, at some intermediate concentration value the total magnetic moment of the system becomes larger than that of pure Ni, resulting in a maximum magnetic moment as a function of Fe content, as shown in Fig. 7. This concentration dependence of magnetic moment of random fcc Fe–Ni alloys agrees with experimental data.[44] At elevated temperatures, magnetic disorder rapidly destroys ferromagnetism for almost all the iron concentrations (Fig. 7), except for the low Fe alloys, where non-vanishing magnetic moment survives up until the Curie transition temperature.

3.3 Magnetism of ordered Fe–Ni compounds

The ordered alloy compounds that we investigated in this paper are $FeNi_3$ with Z1 and $L1_2$ structures, FeNi with $L1_0$ structure, and Fe_3Ni with Z1 and $L1_2$ structures. The $L1_2$ $FeNi_3$ structure plays an important role in the phase diagram of Fe–Ni, being ferromagnetic up to 940 K according to experiment.[45] FeNi with $L1_0$ structure (tetrataenite) is found in meteorites[13–15] and, according to DFT calculations, has the lowest energy of all the alloy configurations with the same stoichiometry. For Fe_3Ni, until recently the $L1_2$ superlattice was believed to have the lowest energy among ordered structures.[46] However, it was found recently by Barabash *et al.*[27] that the Z1 superlattice is more stable than the $L1_2$ structure. In any case, the energies of these structures are fairly close and this prompted us to investigate both of them.

In the absence of constraints on the directions of magnetic moments, four out of the five ordered structures studied here ($L1_0$ FeNi, Z1 Fe_3Ni and both $FeNi_3$ and Fe_3Ni with $L1_2$ structure) are ferromagnetic at low temperatures. The magnetic moments of these structures are shown in Fig. 7. We note here that agreement between magnetic moments predicted for these ordered structures and the experimental observations by Crangle and Hallam[44] is even better than that found for the random structures. The total magnetic moment increases in the Ni-rich part of the concentration range almost linearly as a function of Fe concentration.

In the $L1_2$ Fe_3Ni alloy structure, ferromagnetism is non-collinear, while in other structures the magnetic order is almost exactly collinear. It is important to mention that the energies of collinear and non-collinear magnetic structures of Fe_3Ni are very close, and the two-stage quenching (from 1000 K to 1 K and from 1 K to 0.001 K), with 130 000 attempts per atom at each stage, was necessary to reach the ground state. We did not study the temperature dependence of magnetic properties of the Z1 $FeNi_3$ superlattice, because its energy is about 22 meV per atom higher than that of the $L1_2$ $FeNi_3$ structure. In Fig. 8a we show the temperature dependence of magnetic moment found for the other three ferromagnetic compounds. Similarly to the case of

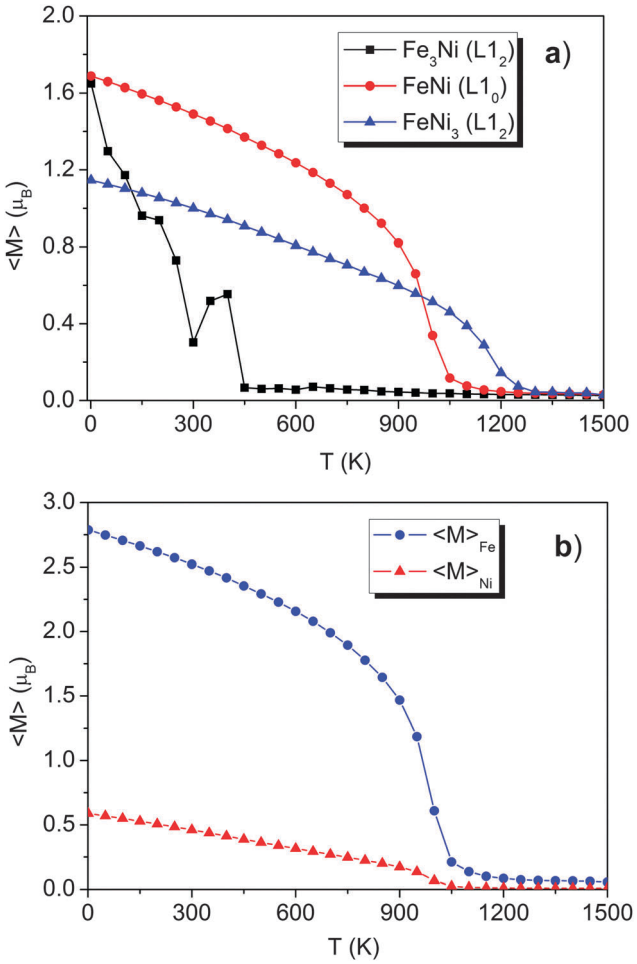

Fig. 8 (a) Temperature dependence of magnetic moments predicted for several ordered fcc Fe–Ni compounds. (b) Magnetic moments of Fe and Ni sublattices in an ordered fcc $L1_0$ FeNi alloy plotted as a function of temperature.

random Fe–Ni mixtures, the total magnetic moment is the highest in FeNi, although it is still close to that of Fe_3Ni. The fact that the energies of collinear and non-collinear magnetic structures are similar in the low Ni concentration range results in relatively strong thermal fluctuations of the overall magnetic moment in $L1_2$ Fe_3Ni structure, as seen in Fig. 8a.

In our simulations the energy of the Z1 Fe_3Ni structure is found to be approximately 9 meV per atom higher than the energy of the $L1_2$ structure. This value is within the error-bar of values predicted by MCE simulations. The Z1 Fe_3Ni superlattice is non-collinear antiferromagnetic, which indicates that its magnetic structure is related to that of the ground state of pure fcc Fe. The main structural difference between the Z1 and $L1_2$ structures is that in Z1 iron and nickel atoms are packed in planes, with a Ni plane followed by three Fe planes. In the $L1_2$ structure, there are alternating Fe and Fe–Ni planes, so that the Z1 superlattice is more segregated, and contains larger volumes of pure Fe. In our opinion, this segregation of Fe and Ni is the main reason explaining the occurrence of non-collinear antiferromagnetism in Z1, whereas in the more mixed $L1_2$, as well as in a random Fe–Ni mixture with the same composition, ferromagnetic non-collinear order is prevalent. It is worth noting that if Monte Carlo simulations are restricted to collinear magnetism, the Z1 structure is also found to be ferromagnetic at low temperatures, with the moments of Fe and Ni atoms being parallel. The energy of a collinear ferromagnetic Z1 structure is 6.5 meV per atom higher than the energy of a non-collinear antiferromagnetic configuration. The average magnitude of magnetic moment of Fe equals 2.645 μ_B, which is very close to that of pure fcc Fe. This agrees with our DFT results, which also predict the magnetic moment of iron in ferromagnetic Z1 structure to be greater than 2.5 μ_B. We believe that antiferromagnetic order can be destroyed more easily by the relatively small additions of Ni in the case of collinear magnetism because the nearly collinear antiferromagnetic fcc Fe structures have energies closer to ferromagnetic fcc Fe than the non-collinear antiferromagnetic fcc Fe configurations.

Of the three ferromagnetic structures studied, temperature fluctuations destroy magnetic order first in $L1_2$ Fe_3Ni, where it vanishes at 450 K (Fig. 8a). FeNi and $FeNi_3$ remain magnetically ordered up to fairly high temperatures of ~1000 K and ~1200 K, respectively. In $FeNi_3$ the predicted Curie temperature is higher than the experimentally observed one. However, as was noted in ref. 47, the experimental Curie point at these high temperatures is an underestimation because of fast self-diffusion and the resulting difficulties associated with maintaining chemical order. For comparison, in a random mixture with $FeNi_3$ composition magnetic order vanishes at 500–550 K whereas in a random mixture with FeNi composition the corresponding temperature is 400–450 K.

The magnetic interaction between Fe and Ni results in both elements retaining magnetic order until the Curie point, as can be observed for ordered FeNi in Fig. 8b. Magnetic order is retained at temperatures much higher than the Curie point in pure Ni for both nickel and iron constituents. This behaviour is similar to that characterizing the magnetization of layers of chromium at the interface with Fe, where the magnetic moment of several atomic layers remains non-zero well above the Néel temperature of Cr.[36]

4. Phase diagram of Fe–Ni alloys

Using the parameters described above, we performed Monte Carlo simulations to establish the equilibrium phase diagram at the interface between bcc and fcc phases. The solubility of Ni in bcc iron is extremely low, with the experimental phase diagram predicting an approximately 5 at% Ni solubility limit at about 800 K, and even smaller values at lower temperatures. Hence the free energy of the bcc Fe–Ni system can be approximated by the free energy of pure bcc iron. Calculations of the free energy of bcc Fe and the difference between bcc and fcc Fe free energies were performed in our previous work, where we predicted the occurrence of bcc–fcc phase transitions in Fe and Fe–Cr, corresponding to the γ-loop in the phase diagram.[9] Using those results and the new data for fcc Fe–Ni, the usual

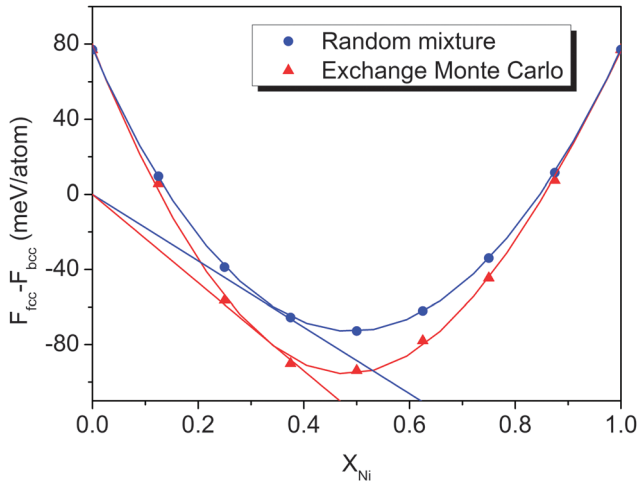

Fig. 9 Tangent construction defining the coexistence curve between bcc Fe and fcc Fe–Ni alloys at temperature T = 600 K.

tangent construction can be applied to evaluate the coexistence curve. An example of such construction for T = 600 K is given in Fig. 9. As discussed in Section 2, we performed two separate calculations for the Fe–Ni system: one for a random mixture and another for a case where atomic exchanges were included. We found that the free energy of a random mixture was always lower than the enthalpy of mixing of a system where atoms were allowed to exchange. This was observed for all the temperatures and concentrations studied here. In order to provide the lower estimate for the free energy, we added the ideal configuration entropy (3) to the enthalpy of the alloy system where exchanges were permitted. The two tangent constructions gave almost identical results for the bcc–fcc coexistence curve, as can be seen in Fig. 9 and 10. The predicted coexistence curve (Fig. 10) shows that the area of the phase diagram where fcc Fe–Ni alloys are stable, is very broad, in agreement with experimental data.[12] Note that our calculations do not take into account lattice

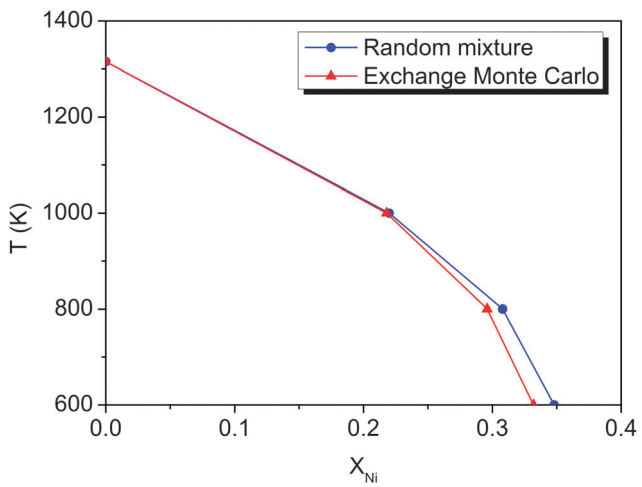

Fig. 10 Coexistence curves between bcc Fe and fcc Fe–Ni alloys. The blue line corresponds to random alloys, the red line was computed using exchange Monte Carlo simulations.

vibrations. This approximation is well justified for the case of Fe–Ni alloys, where the atomic radii of the two elements are similar and the vibrational entropy of alloying is very low. In a study by Bogdanoff and Fultz,[48] based on the experimental information about the phonon density of states, the vibrational entropy of alloying was found to be $\Delta S_{vib}^{alloy} = 0.02\ k_B$ per atom for the $FeNi_3$ compound with $L1_2$ structure, which is smaller than the error-bar of $\pm 0.03\ k_B$ per atom, and much smaller than the ideal configurational entropy, which is 0.562 k_B per atom at that composition. It is interesting to note here that a recent *ab initio* study found that despite quite large individual ionic displacements in the Invar concentration range ($Fe_{65}Ni_{35}$),[49] the influence of local lattice relaxation on the energy of Fe–Ni alloy configurations was small. One of the authors of ref. 49 specifically relates this to the small mismatch between the sizes of Fe and Ni atoms in a subsequent study,[50] in agreement with our findings. In other words, the lattice contribution to the free energy can indeed be neglected over a broad range of alloy compositions.

In the high-Ni part of the phase diagram, it is necessary to compare the energies of ordered structures ($L1_2$ for the case of $FeNi_3$ and $L1_0$ for the case of FeNi) with the free energies of random mixtures computed for the same alloy compositions. For the ordered structures, the configuration entropy is zero. For the random mixtures, we again used expression (3) for the ideal configuration entropy. The free energies of ordered and random systems are compared in Fig. 11. For FeNi, random structures become more energetically favourable at about 520 K, whereas for the $FeNi_3$ compound, at about 730 K. These numbers should be compared with experimental temperatures of 593 K and 770 K, respectively.[51,52] The small underestimation of the order–disorder transition temperatures compared to experiment can be related to the fact that the actual configuration entropy is slightly higher than the ideal one because of the remaining order in the structures at low temperatures. Summarizing these results, we conclude that while the ordered $FeNi_3$ system is certainly stable until high enough temperatures, for the FeNi $L1_0$ structure the temperature of the order–disorder transformation is relatively low, meaning that it might take a very long time for the alloy of that composition to reach the ordered state during cooling. Combining transition temperatures for the ordered ferromagnetic and disordered antiferromagnetic systems (520 K and 730 K) with the Curie temperature of Ni, which our simulations predict to be 550–600 K, we are able to explain the experimentally observed maximum of magnetic transformation temperature found as a function of nickel content.

5. Discussion

The effect of magnetism on the thermodynamic properties of solids and structural phase transitions has long been recognized. For example, the ferromagnetic–paramagnetic transition in iron at 1043 K is responsible for the bcc–fcc transition at 1185 K.[9,53,54] Recent advances in simulation algorithms expanded the range of systems accessible to simulation from

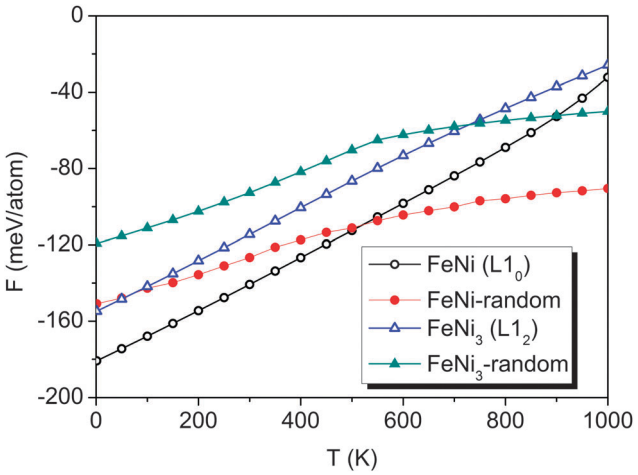

Fig. 11 Comparison of free energies of ordered and random structures simulated using MCE for stoichiometric compositions of fcc FeNi and $FeNi_3$.

pure metals to binary alloy solutions with different degrees of chemical disorder. In this paper, we show how magnetic cluster expansion can be applied to magnetic fcc Fe–Ni alloys.

The main difference between the phase diagram of Fe–Cr studied earlier and Fe–Ni alloys is the fact that the area of the phase diagram, where fcc structure is stable, is very large. The so-called γ-loop in the Fe–Cr phase diagram extends up to ~14 at% Cr, while in Fe–Ni the fcc structure is more stable than bcc for almost all the concentrations and temperatures. This is the consequence of strong ferromagnetic interactions between iron and nickel in the fcc phase resulting in large negative energies of mixing seen in *ab initio* calculations. Our parameterization of MCE Hamiltonian also predicts a strong ferromagnetic exchange coupling between the second and third nearest Fe–Ni neighbours and negative enthalpy of mixing, in excess of −100 meV per atom, even for the random alloy configurations. The magnetic behaviour of random alloy configurations is characterized by a transition from non-collinear antiferromagnetism on the iron-rich side to collinear ferromagnetism on the nickel-rich side of the concentration range. The large magnetic moment of Fe, compared to Ni, results in a maximum total magnetic moment of the system as a function of concentration. At elevated temperatures, magnetic order vanishes first at the Fe-rich side of the concentration range. At the nickel-rich side, our calculations predict collinear ferromagnetism for the high-Ni random structures and for several ordered superlattices with Ni content of 50 at% and higher. The magnetic moment of the system increases linearly as a function of Fe content and has a maximum, in full agreement with experimental data,[44] particularly for the ordered structures.

The temperature dependence of magnetism in several ferromagnetically ordered intermetallic compounds was also studied. While the magnetic order in the $L1_2$ superlattice of Fe_3Ni vanishes at relatively low temperatures, FeNi and $FeNi_3$ remain ferromagnetic even above 1000 K. In fact this is the main reason why they become unstable with respect to transformation into chemically disordered configurations. The Curie temperatures for random alloy mixtures are much lower than those for the ordered structures, and above the corresponding Curie temperatures the disordered configurations are paramagnetic. It is well known that in the paramagnetic state the magnetic energy increases with temperature much more slowly than in a ferromagnetic state (Fig. 11), hence at higher temperatures an ordered compound becomes less energetically favourable than a random alloy mixture. It is worth noting here that one previous theoretical study of order–disorder phenomena in Fe_3Ni, FeNi, and $FeNi_3$[47] found magnetic order even in chemically disordered alloys at temperatures where they are more stable than the ordered ones. The study was based on an Ising Hamiltonian, which appears to be unrealistic for the fairly magnetically directionally isotropic Fe–Ni alloys. Our calculations also show that in the limit of a strongly magnetically anisotropic MCE Hamiltonian, a chemically disordered system remain ferromagnetic until higher temperatures. However, an experimental study[55] found only small magnetic crystal anisotropy in iron–nickel alloys. Recent work by Ekholm *et al.*[56] successfully explained the existence of magnetic order in chemically disordered $FeNi_3$ using cluster expansion Hamiltonian with parameters depending on alloy composition and the total magnetization of the system. Still, in their approach magnetic and chemical degrees of freedom were treated separately, and the cluster expansion parameters obtained from a completely disordered system were used for modelling a system just above the order–disorder transition, which inevitably has significant short-range order. We believe that a realistic Hamiltonian for that system should be almost entirely isotropic, and includes chemical and magnetic degrees of freedom on equal footing as in the present approach. The question of interplay between chemical and magnetic order–disorder transitions is very complicated, and the possibility that some magnetic order above the chemical order–disorder transition may be related to precipitates of ordered phases or to short-range chemical order remaining at temperatures where long-range chemical order is already absent deserves further attention.

For the Z1 Fe_3Ni superlattice, non-collinear antiferromagnetic order is predicted. It is reasonable to expect that other antiferromagnetic ordered structures may also exist in the region of high Fe concentration, with their magnetic structures similar to those of pure fcc iron. The energies of Z1 and $L1_2$ structures in Fe_3Ni are found to be close to each other. Also, DFT calculations performed for several different structures with 25 at% Ni content predict fairly similar energies. These structures can be either completely ferromagnetic or partially antiferromagnetic (ferrimagnetic), with some of the Fe atoms having magnetic moment directions opposite to the rest of the moments, without involving a large penalty in energy. The volumes of these structures as calculated by DFT differ by 2–3% (with ferrimagnetically ordered systems having a smaller volume) – an effect which cannot be modelled using the current rigid lattice MCE approach. This abundance of superlattices and magnetic structures within a narrow energy range is in agreement with previous calculations[24] that relate the occurrence of the ferrimagnetic phase to the Invar effect at around 35 at% Ni. Our MCE calculations exploring several superlattices

with Fe_2Ni composition found ferromagnetic as well as ferrimagnetic ground states, but the energy of the antiferromagnetic configuration seems too high and cannot be obtained without constraining the total magnetic moment of the system. Another possible reason explaining the Invar effect, the non-collinearity of magnetic structures,[57] has also been observed in our simulations for both the ordered (Z1) and random Fe–Ni mixtures with Ni content not exceeding that of Fe.

The model developed above is limited to the classic Heisenberg–Landau-like Hamiltonians. Recent studies on pure Fe and Cr[58,59] showed the significance of taking quantum corrections and lattice anharmonicity into account at high temperatures, to achieve fully quantitative description of the phase diagram. Still, the methodology proposed in ref. 58 and 59 is yet to be extended to solid solutions of metals. In our previous work,[9] by taking into account vibrational contributions to the free energy, we correctly estimated the size of the γ-loop in Fe–Cr, but were only able to do that in a narrow range of Cr concentrations not exceeding 15 at% Cr. For the fcc Fe–Ni alloy studied here, the vibrational contribution to the free energy is small,[48,50] and the current parameterization of the MCE Hamiltonian without quantum and vibrational corrections made it possible to undertake a realistic study of magnetic and thermodynamic properties of the alloy in a broad range of temperatures and concentrations. Good agreement with experiment was found for the fcc–bcc coexistence curve in the phase diagram and for the temperatures of order–disorder transitions in FeNi and $FeNi_3$ compounds. This confirms that the MCE model is now ready to be extended to the ternary Fe–Ni–Cr alloy.

Acknowledgements

This work was part-funded by the RCUK Energy Programme (Grant Number EP/I501045) and by the European Union's Horizon 2020 research and innovation programme under grant agreement number 633053. To obtain further information on the data and models underlying this paper please contact PublicationsManager@ccfe.ac.uk. The views and opinions expressed herein do not necessarily reflect those of the European Commission. This work was also part-funded by the United Kingdom Engineering and Physical Sciences Research Council *via* a programme grant EP/G050031. DNM would like to thank Jülich supercomputer centre for using the High-Performances Computer for Fusion (HPC-FF) facilities as well as the International Fusion Energy Research Centre (IFERC) for using the supercomputer (Helios) at Computational Simulation Centre (CSC) in Rokkasho (Japan). JSW was supported by the Accelerated Metallurgy Project, which was co-funded by the European Commission in the 7th Framework Programme (Contract NMP4-LA-2011-263206), the European Space Agency and individual partner organisations. The authors are grateful to the referees for their helpful and stimulating comments.

References

1 S. L. Dudarev, *et al.*, *J. Nucl. Mater.*, 2009, **386–388**, 1.
2 T. Toyama, *et al.*, *J. Nucl. Mater.*, 2012, **425**, 71.
3 D. Terentyev and A. Bakaev, *J. Nucl. Mater.*, 2013, **442**, 208.
4 R. Meyer and P. Entel, *Phys. Rev. B: Condens. Matter Mater. Phys.*, 1998, **57**, 5140.
5 Y. Mishin, M. J. Mehl and D. A. Papaconstantopoulos, *Acta Mater.*, 2005, **53**, 4029.
6 G. Bonny, R. C. Pasianot and L. Malerba, *Modell. Simul. Mater. Sci. Eng.*, 2009, **17**, 025010.
7 G. Bonny, R. C. Pasianot and L. Malerba, *Philos. Mag.*, 2009, **89**, 3451.
8 M. Yu. Lavrentiev, S. L. Dudarev and D. Nguyen-Manh, *J. Nucl. Mater.*, 2009, **386–388**, 22.
9 M. Yu. Lavrentiev, D. Nguyen-Manh and S. L. Dudarev, *Phys. Rev. B: Condens. Matter Mater. Phys.*, 2010, **81**, 184202.
10 M. Yu. Lavrentiev, D. Nguyen-Manh and S. L. Dudarev, *Comput. Mater. Sci.*, 2010, **49**, S199.
11 M. Yu. Lavrentiev, S. L. Dudarev and D. Nguyen-Manh, *J. Appl. Phys.*, 2011, **109**, 07E123.
12 V. I. L. J. Swartzendruber and C. Alcock, *Phase Diagrams of Binary Iron Alloys*, ASM International, Materials Park, OH, 1993.
13 J. F. Albertsen, G. B. Jensen and J. M. Knudsen, *Nature*, 1978, **273**, 453.
14 R. S. Clarke Jr. and E. R. D. Scott, *Am. Mineral.*, 1980, **65**, 624.
15 C.-W. Yang, D. B. Williams and J. I. Goldstein, *Geochim. Cosmochim. Acta*, 1997, **61**, 2943.
16 M. Yu. Lavrentiev, D. Nguyen-Manh and S. L. Dudarev, *Solid State Phenom.*, 2011, **172–174**, 1002.
17 Y. Zhang, *et al.*, *Prog. Mater. Sci.*, 2014, **61**, 1.
18 P. E. Blöchl, *Phys. Rev. B: Condens. Matter Mater. Phys.*, 1994, **50**, 17953.
19 G. Kresse and J. Hafner, *Phys. Rev. B: Condens. Matter Mater. Phys.*, 1994, **49**, 14251.
20 G. Kresse and J. Furthmüller, *Comput. Mater. Sci.*, 1996, **6**, 15.
21 G. Kresse and J. Furthmüller, *Phys. Rev. B: Condens. Matter Mater. Phys.*, 1996, **54**, 11169.
22 J. P. Perdew, K. Burke and M. Ernzerhof, *Phys. Rev. Lett.*, 1996, **77**, 3865.
23 A. V. Ruban, *et al.*, *Phys. Rev. B: Condens. Matter Mater. Phys.*, 2005, **71**, 054402.
24 I. A. Abrikosov, *et al.*, *Phys. Rev. B: Condens. Matter Mater. Phys.*, 2007, **76**, 014434.
25 J. M. Sanchez, F. Ducastelle and D. Gratias, *Physica A*, 1984, **128**, 334.
26 V. Blum, *et al.*, *Phys. Rev. B: Condens. Matter Mater. Phys.*, 2005, **72**, 165113.
27 S. V. Barabash, *et al.*, *Phys. Rev. B: Condens. Matter Mater. Phys.*, 2009, **80**, 220201.
28 H. Wang, *et al.*, *Phys. Chem. Chem. Phys.*, 2013, **15**, 7599.
29 M. Yu. Lavrentiev, *et al.*, *J. Phys. Chem. B*, 2001, **105**, 3594.
30 F. M. Marquez, *et al.*, *Modell. Simul. Mater. Sci. Eng.*, 2003, **11**, 115.
31 M. Yu. Lavrentiev, J. A. Purton and N. L. Allan, *Am. Mineral.*, 2003, **88**, 1522.
32 M. Yu. Lavrentiev, N. L. Allan and J. A. Purton, *Phys. Chem. Chem. Phys.*, 2003, **5**, 2190.
33 M. Yu. Lavrentiev, *et al.*, *Phys. Rev. B: Condens. Matter Mater. Phys.*, 2007, **75**, 014208.

34 Y. Tsunoda, *J. Phys.: Condens. Matter*, 1989, **1**, 10427.
35 A. Onodera, *et al.*, *Phys. Rev. B: Condens. Matter Mater. Phys.*, 1994, **50**, 3532.
36 M. Yu. Lavrentiev, *et al.*, *Phys. Rev. B: Condens. Matter Mater. Phys.*, 2011, **84**, 144203.
37 Q. Chen and B. Sundman, *J. Phase Equilib.*, 2001, **22**, 631.
38 S. Blundell, *Magnetism in Condensed Matter*, Oxford University Press, 2001.
39 P. Yu, *et al.*, *Phys. Rev. B: Condens. Matter Mater. Phys.*, 2008, **77**, 054431.
40 J. Kudrnovsky, V. Drchal and P. Bruno, *Phys. Rev. B: Condens. Matter Mater. Phys.*, 2008, **77**, 224422.
41 R. Idczak, R. Konieczny and J. Chojcan, *Physica B*, 2012, **407**, 235.
42 G. Cacciamani, *et al.*, *Intermetallics*, 2010, **18**, 1148.
43 W. Xiong, *et al.*, *Acta Mater.*, 2011, **59**, 521.
44 J. Crangle and G. C. Hallam, *Proc. R. Soc. London, Ser. A*, 1963, **272**, 119.
45 R. J. Wakelin and E. L. Yates, *Proc. R. Soc. London, Ser. B*, 1953, **66**, 221.
46 T. Mohri and Y. Chen, *J. Alloys Compd.*, 2004, **383**, 23.
47 M. Z. Dang and D. G. Rancourt, *Phys. Rev. B: Condens. Matter Mater. Phys.*, 1996, **53**, 2291.
48 P. D. Bogdanoff and B. Fultz, *Philos. Mag. B*, 1999, **79**, 753.
49 F. Liot and I. A. Abrikosov, *Phys. Rev. B: Condens. Matter Mater. Phys.*, 2009, **79**, 014202.
50 M. Ekholm, *et al.*, *Phys. Rev. Lett.*, 2010, **105**, 167208.
51 J. Paulevé, *et al.*, *C. R. Acad. Sci.*, 1962, **254**, 965.
52 J. W. Drijver, F. van der Woude and S. Radelaar, *Phys. Rev. Lett.*, 1975, **34**, 1026.
53 I. Leonov, *et al.*, *Phys. Rev. Lett.*, 2011, **106**, 106405.
54 F. Körmann, *et al.*, *Phys. Status Solidi B*, 2014, **251**, 53.
55 R. M. Bozorth and J. G. Walker, *Phys. Rev.*, 1953, **89**, 624.
56 M. Ekholm, *et al.*, *Phys. Rev. Lett.*, 2010, **105**, 167208.
57 M. van Schilfgaarde, I. A. Abrikosov and B. Johansson, *Nature*, 1999, **400**, 46.
58 F. Körmann, *et al.*, *Phys. Rev. B: Condens. Matter Mater. Phys.*, 2010, **81**, 134425.
59 F. Körmann, *et al.*, *J. Phys.: Condens. Matter*, 2013, **25**, 425401.